

# Magnetically Actuated Reconfigurable Metamaterials as Conformal Electromagnetic Filters

Shuai Wu, Jack Eichenberger, Jize Dai, Yilong Chang, Nima Ghalichechian, and Ruike Renee Zhao\*

Electromagnetic (EM) metamaterials with tailored properties are developed for wave manipulation, filtering, and cloaking for aerospace and defense applications. While traditional EM metamaterials exhibit fixed behaviors due to unchangeable material properties and geometries after fabrication, reconfigurable EM metamaterials allow for tunable performance through electrical/mechanical reconfiguration strategies. Traditional biasing circuit-based electrical reconfiguration poses challenges due to complex circuit design, while motor-driven mechanical reconfiguration can lead to bulky and tethered structures with restricted adaptability. Herein, magnetically actuated structurally reconfigurable EM metamaterials with enhanced adaptability/conformability to different geometries, showing merits of fast, reversible, and programmable shape morphing, are developed. Magnetic actuation enables metamaterial's mechanical reconfiguration between flat deployed, flat folded, curved deployed, and curved folded states for both conformal and freestanding 3D shape morphing. Locally, the EM metamaterials fold subwavelength units for tunable properties, switching between all-pass and band-stop behaviors upon structural reconfiguration. Globally, the structure can conform and morph to different curved surfaces. The structurally reconfigurable metamaterial also serves as a medium for customizable subwavelength units by rationally designing attached conductive patterns for varied filtering performances such as narrow-band, dual-band, and wide-band filtering behaviors, illustrating the design flexibility and application versatility of the developed structurally reconfigurable EM metamaterial.

patterns, showing tailorable mechanical,<sup>[1]</sup> acoustic,<sup>[2]</sup> optical,<sup>[3]</sup> or electromagnetic (EM)<sup>[4]</sup> properties that are beneficial for diverse functions including noise control,<sup>[5]</sup> vibration isolation,<sup>[6]</sup> EM wave manipulation,<sup>[7]</sup> cloaking,<sup>[8]</sup> energy harvesting,<sup>[9]</sup> etc. For example, EM metamaterials are capable of manipulating EM waves due to their constructed subwavelength units, whose dimension, geometry, and arrangement decide the performance of the metamaterial. They have been demonstrated as reflectors, filters, polarizers, or antennas with enhanced gain and bandwidth.<sup>[10]</sup> However, traditional EM metamaterials only exhibit fixed behaviors during operation due to unchangeable geometries and materials once fabricated. Alternatively, reconfigurable metamaterials, also called active metamaterials, possess actively tunable patterns and/or physical properties, facilitating more versatile and programmable use.<sup>[11]</sup> Tunable EM properties of the metamaterials are usually achieved by either electrical or structural reconfiguration through different strategies such as programming biasing circuits or reshaping the subwavelength units, respectively.<sup>[12]</sup>

## 1. Introduction


Metamaterials, in which “meta” means “beyond,” are architected structures exhibiting physical properties that are not present in nature. Metamaterials consist of specifically designed periodic

Electrical reconfiguration by introducing unit variability, typically achieved via p–i–n diodes or varactor diodes, is a conventional method that allows for real-time tuning and precise control of the EM performance of the metamaterial. For instance, wave polarization is controlled via switching probes<sup>[13]</sup> and

S. Wu, J. Dai, Y. Chang, R. R. Zhao  
Department of Mechanical Engineering  
Stanford University  
Stanford, CA 94305, USA  
E-mail: rrzhuo@stanford.edu

J. Eichenberger  
Department of Electrical and Computer Engineering  
The Ohio State University  
Columbus, OH 43212, USA

N. Ghalichechian  
School of Electrical and Computer Engineering  
Georgia Institute of Technology  
Atlanta, GA 30332, USA

 The ORCID identification number(s) for the author(s) of this article can be found under <https://doi.org/10.1002/aisy.202200106>.

© 2022 The Authors. Advanced Intelligent Systems published by Wiley-VCH GmbH. This is an open access article under the terms of the Creative Commons Attribution License, which permits use, distribution and reproduction in any medium, provided the original work is properly cited.

DOI: 10.1002/aisy.202200106

varactor diodes,<sup>[14]</sup> and wave reflection/transmission states are manipulated with p–i–n diodes.<sup>[15]</sup> However, biasing circuits and extra conductive components of the electrical reconfiguration can affect the metamaterial EM performance negatively. Large-scale metamaterials also become increasingly complex to fabricate as more electrical components and a more extensive biasing circuit are needed. Furthermore, the fabrication of p–i–n diodes and varactor diodes by printed circuit boards (PCBs) generally leads to rigid structures, which limits the metamaterials' capability to pack, deploy, or conform to curved surfaces that are very common in defense and aerospace applications.

Structural reconfiguration is an alternative method to tune EM metamaterials' properties through material phase change,<sup>[16]</sup> translational/rotational behavior,<sup>[17]</sup> and shape morphing<sup>[18]</sup> of structures. Herein, appropriately designed materials, structures, and actuation methods are essential to reshape or rearrange subwavelength units and shift the metamaterial's properties in a controllable manner. For example, EM metamaterials relying on origami/kirigami folding<sup>[19]</sup> and structural buckling<sup>[20]</sup> have been developed for reconfigurable antennas. In these systems, shape morphing and the coupled property reconfiguration are driven by manual handling, motors, or pumps, which can lead to bulky and tethered structures with restricted reliability, flexibility, and versatility. Magnetically responsive metamaterials<sup>[21]</sup> provide robust alternative strategies for reconfigurable EM metamaterials by structurally reshaping the metamaterial system under the applied magnetic field. They show advantages of selective, programmable, and reversible actuation while possessing the merits of fast and untethered control.<sup>[22]</sup> In this work, we develop structurally reconfigurable EM metamaterials by constructing magnetically actuated planar lattices that can locally fold the subwavelength units for tunable EM properties and globally morph between flat and curved configurations as conformal and 3D freestanding metamaterials (**Figure 1**).

In the following sections, we first introduce how magnetic actuation drives metamaterial's structural reconfiguration between flat deployed, flat folded, curved deployed, and curved folded states for both conformal and freestanding 3D shape morphing. The reconfigurations are predicted and guided by structural finite element analysis (FEA) and verified experimentally. Then, based on the EM full-wave simulation, subwavelength units are constructed by attaching the structural units with rationally designed conductive patterns, realizing EM metamaterials with actively tunable properties as filters. In both EM simulation and experimental measurement, the EM metamaterials switch between all-pass and band-stop upon magnetic reconfiguration. Finally, by customizing conductive patterns, varied EM filtering effects are demonstrated with different frequencies and bandwidths under the guidance of EM simulation.

## 2. Results

### 2.1. Magnetic Actuation of the Structurally Reconfigurable Metamaterial

As shown in Figure 1A, we adopt a 2D unit design with eight blocks of magnetic soft composites connected by hinges highlighted in blue. Both the blocks and hinges are magnetic composites

fabricated by molding (Figure S1, Supporting Information). To realize shape reconfiguration, the unit is programmed with alternating magnetization directions denoted by the white arrows. Upon an in-plane magnetic field  $B$  perpendicular to the initial magnetization directions, the neighboring blocks rotate in reverse directions and tend to align their magnetizations with  $B$ . We define the initial square-shaped configuration as the deployed state and the deformed star-shaped configuration as the folded state. The shape reconfiguration of the magnetic unit is induced by the elastic deformation of thin hinges and the rigid body rotation of magnetic blocks. After switching off the applied magnetic field  $B$ , the stored elastic energy in the hinges releases, and the magnetic unit instantly recovers to the initial deployed state. As the effective magnetic actuation of the metamaterial relies on rationally designed dimensions of the magnetic blocks and hinges, structural FEA is utilized to simulate the folding of the metamaterial under the applied magnetic field (see Experimental Section for structural FEA details) to guide the unit design (Figure S1, Supporting Information).

Assembling the units yields a planar magnetic lattice (see Figure S2, Supporting Information, for the detailed magnetizing and assembling process). The metamaterial switches between the flat deployed state (Figure 1B) and the flat folded state (Figure 1C) under the magnetic field. Here, each magnetic unit exhibits local folding deformation, as illustrated in the red box, accumulatively leading to a denser global configuration of the metamaterial. The structural FEA prediction agrees with experimental validation (Video 1). A pair of customized single-axis Helmholtz coils is used to generate a homogeneous magnetic field for the magnetic actuation of metamaterial in this work (Figure S3, Supporting Information). The planar metamaterial's lattice feature enables its structural flexibility and allows it to morph to a 3D curved state, as demonstrated in Figure 1D. The metamaterial can conform to a curved substrate under gravity or adhesion. It can then reconfigure to the curved folded state (Figure 1E) under magnetic field while maintaining its curvature. Note that by programming the magnetization distribution, the metamaterial can directly morph to the curved folded state (Figure 1E) from the flat deployed state (Figure 1B) without the presence of a substrate (details will be discussed in the later section). Taking advantage of structural reconfigurability, EM metamaterials can be constructed by incorporating conductive patterns onto the surface, functioning as subwavelength units as illustrated in Figure 1F. Here, the metamaterial serves as the medium for structural reconfiguration of the subwavelength units. By 2D or 3D shape morphing under the magnetic field, the metamaterial rearranges the conductive patterns both locally and globally, leading to programmable EM properties in an on-demand manner. It should be noted that magnetic actuation applies to different scales based on various advanced fabrication techniques. By tuning the geometries and dimensions of the metamaterial, the feature size and distribution of the subwavelength units can be tailored and engineered for the preferred wavelength and application interest.

### 2.2. Reconfigurable Metamaterial Conforming to Different Geometries

To demonstrate the adaptability and conformability of the designed metamaterial on different geometries, structural

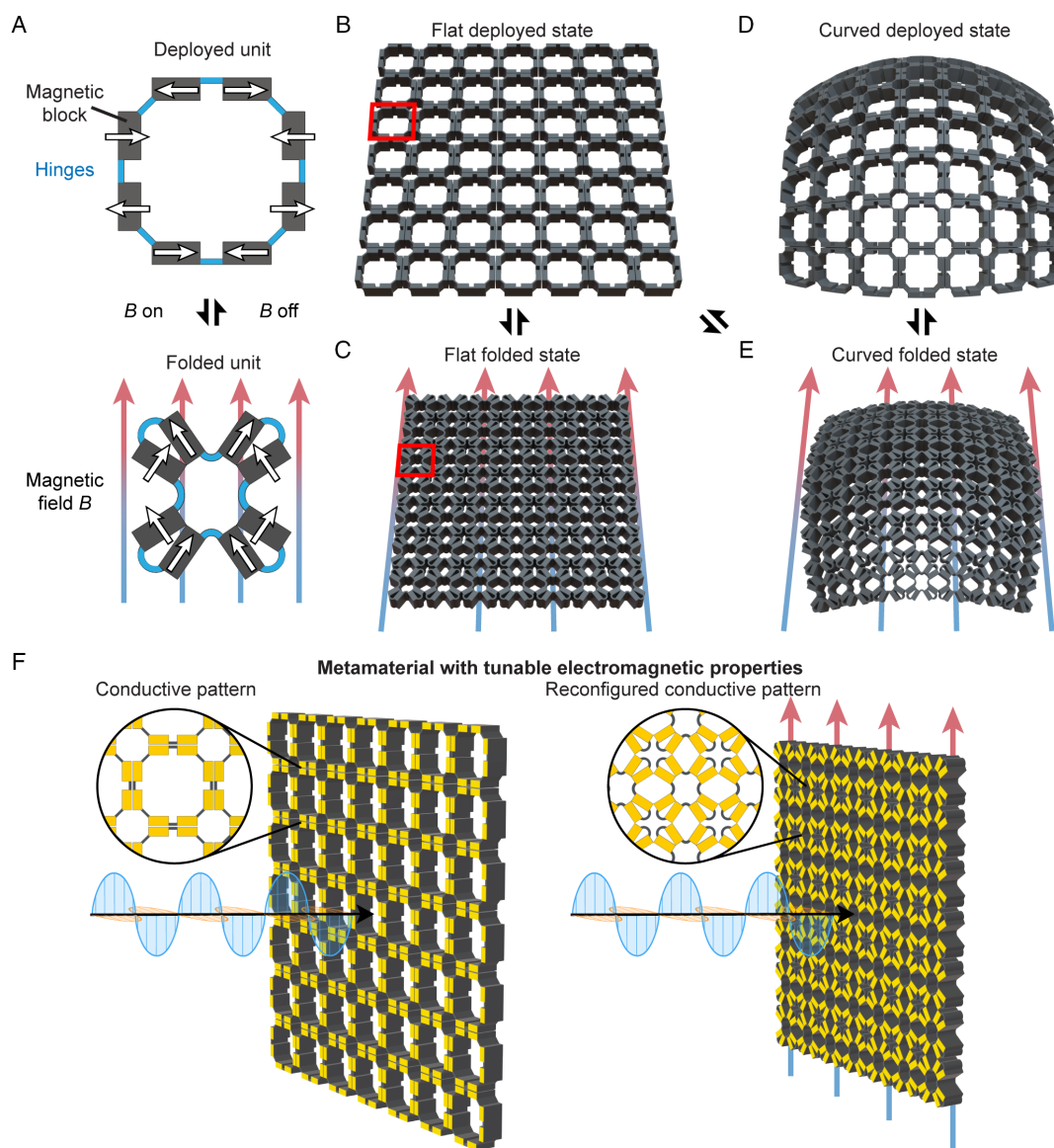


**Figure 1.** Magnetically actuated reconfigurable metamaterial with tunable EM properties. A) Magnetic actuation of a unit switching between the deployed and folded states. The units are assembled into a planar lattice, which morphs between B) the flat deployed state and C) the flat folded state via magnetic actuation. The flexible metamaterial can morph to a 3D structure with D) curved deployed state and E) curved folded state. F) Attaching electrically conductive patterns enables reconfigurable EM metamaterials with actively tunable properties by shape morphing under the applied magnetic field.

reconfiguration of the metamaterial (90 mm by 90 mm by 2 mm) on a cylindrical substrate (radius of 75 mm) is simulated, as shown in **Figure 2A**. From the structural FEA, it is observed that the metamaterial nicely conforms to the curved surface at both deployed and folded states under magnetic actuation, assisted by gravity. **Figure 2B** shows the experimental verification. Under a 60 mT magnetic field, the metamaterial morphs from the deployed state to the folded state on the cylindrical substrate, maintaining conformability. While recovering, a reversing magnetic field of 15 mT is applied to assist a rapid deployment of the metamaterial (**Video 2**). The magnetic actuation permits fast (subseconds), reversible, and untethered deformation locally and globally. As shown by

the structural FEA in **Figure 2C**, the structure also adapts to a spherical substrate (radius of 75 mm) with reversible shape morphing under magnetic actuation. The experimental verification (**Figure 2D** and **Video 3**) shows reliable folding and deploying under the 60 mT magnetic field and 15 mT reversing magnetic field, illustrating decent agreement with the simulated deformations. The metamaterial shows the capability to adapt to geometries with varied sizes (cylindrical and spherical substrates with a radius of 100 mm in **Figure S4**, Supporting Information). The coupled reconfigurability and conformability will enable EM metamaterials with wide property tunability and programmability, which will be discussed in the later sections.

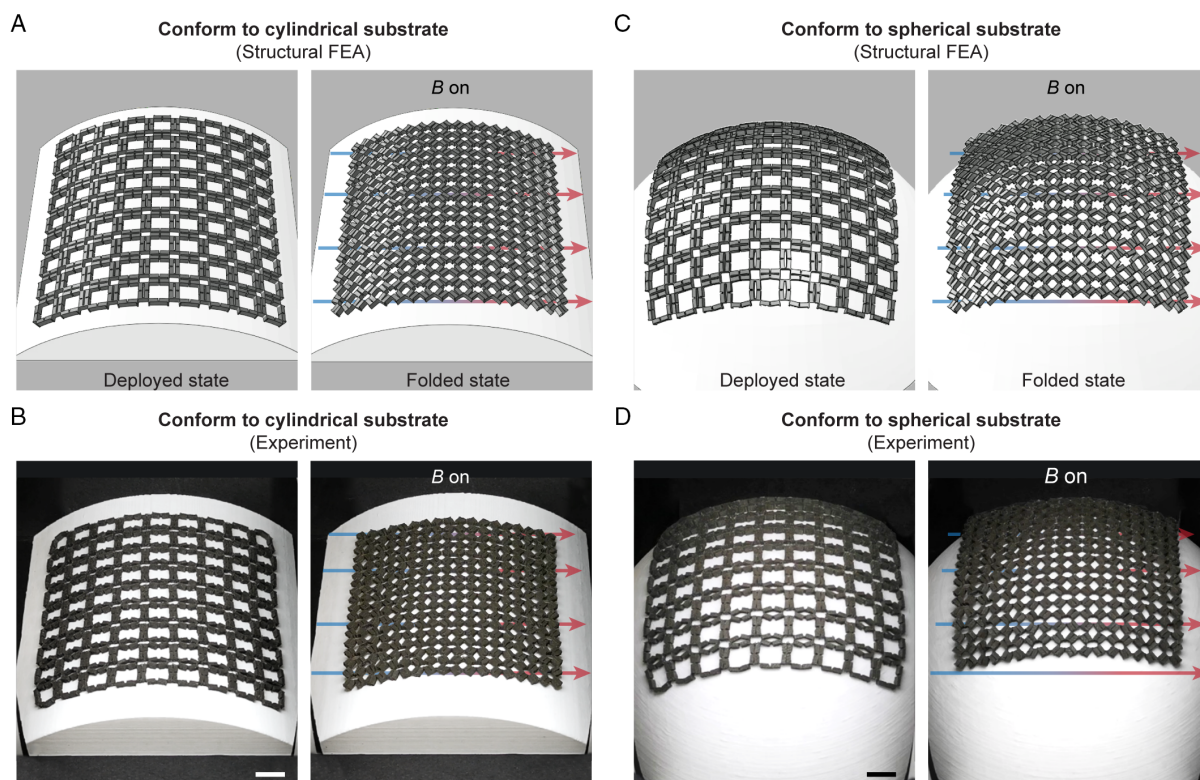


**Figure 2.** Magnetically actuated metamaterial conforms to different geometries. A) Structural FEA prediction and B) experimental validation of the metamaterial at both deployed state and folded state conforming to a cylindrical surface with a radius of 75 mm. C) Structural FEA prediction and D) experimental validation of the metamaterial at both deployed state and folded state conforming to a spherical surface with a radius of 75 mm. Scale bars: 1 cm.

### 2.3. 3D Freestanding Reconfigurable Metamaterial

Apart from conforming to various geometries, the metamaterial is also able to morph into freestanding curved configurations, as demonstrated in **Figure 3**. This provides a robust design strategy that combines both local and global shape morphing capabilities to achieve reconfigurable metamaterials with more degrees of freedom. In this case, magnetic units are designed with both in-plane and out-of-plane magnetization components for local and global deformation, respectively, under magnetic actuation. For the seven-by-seven array demonstrated, locally, each magnetic unit possesses the alternating in-plane magnetization directions along the positive and negative Y-direction (white arrows), as shown by the top view of single unit in **Figure 3A**. Globally, the left three columns of the metamaterial are programmed with the out-of-plane magnetizations with angles of 30°, 45°, 60° to the negative Z-direction, and the right three columns are programmed with angles of 60°, 45°, 30° to the positive Z-direction, as illustrated by the metamaterial side view in **Figure 3B**. The middle column units possess in-plane magnetization only. Under an X-direction magnetic field, the in-plane magnetization folds each magnetic unit locally, and the out-of-plane magnetization drives the planar metamaterial to bend up, forming a freestanding curved configuration. Structural FEA is implemented to predict the magnetic actuation, as shown in **Figure 3C**, demonstrating the shape morphing of the metamaterial from a

flat deployed state to a freestanding curved folded state. Experimental verification of the metamaterial under an increasing homogeneous magnetic field up to 100 mT along the positive X-direction is also carried out as shown in **Figure 3D** and **Video 4**, following the structural FEA prediction well. By applying a reversing magnetic field of 15 mT, the structure instantly recovers to the initial flat deployed state (**Video 4**). **Figure S5**, Supporting Information, provides a detailed magnetization process for fabricating magnetic units with predetermined in-plane and out-of-plane magnetization components. Guided by structural FEA, the out-of-plane magnetization component can be customized for different 3D shape reconfigurations to realize a desired curvature distribution of the metamaterial.

### 2.4. Reconfigurable EM Metamaterials for Tunable EM Properties

The previous sections have demonstrated the magnetically actuated metamaterial with effective structural reconfigurability and conformability enabled by combined local and global shape morphing. The local shape morphing (unit folding) provides the foundation for property tunability of the reconfigurable EM metamaterials, which can be developed by incorporating functional components, namely, subwavelength units, into the mechanical system. These metamaterials could potentially serve

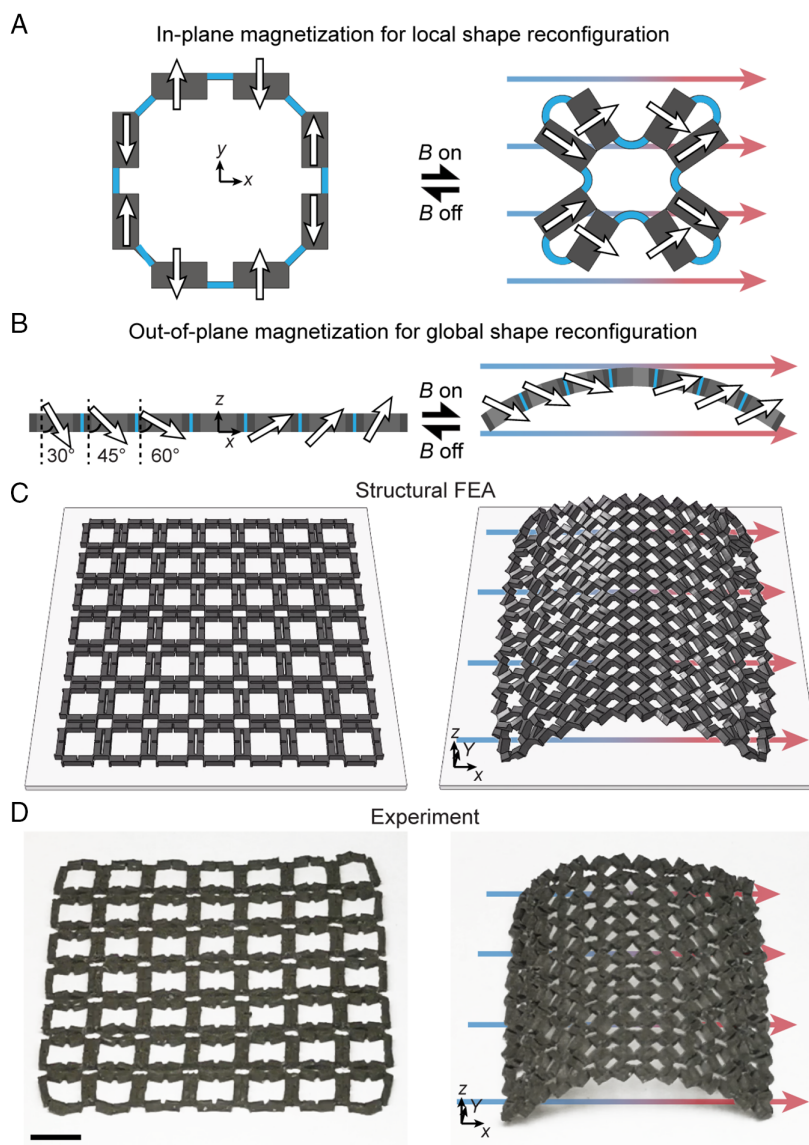


**Figure 3.** Freestanding reconfigurable metamaterial. A) In-plane magnetization distribution for folding of each unit. B) Out-of-plane magnetization distribution for global shape reconfiguration of the metamaterial. C) Structural FEA prediction and D) experimental verification of the magnetically reconfigurable metamaterial for integrated local and global shape morphing. Scale bar: 1 cm.

as waveguides or wave filters with tunable EM properties on the fly. We utilize EM simulation to guide the design of subwavelength units, which is implemented by attaching conductive patterns to the surface of the metamaterial (see details in the Experimental Section). Here, an “S”-shaped pattern is attached to each unit in the metamaterial (dimensions provided in Figure S6, Supporting Information). A  $13 \times 13$  array (approximate size 170 mm by 170 mm) is adopted, which is sufficiently large to represent an infinite metamaterial based on EM full-wave simulation (Figure S7, Supporting Information). In the EM simulation, the metamaterial is positioned between a pair of horn antennas (Figure 4A). The first antenna generates an incident wave as the signal source and the second antenna receives the wave passing through the metamaterial. Upon folding of the flat

metamaterial, the structure reconfigures from a band-stop filter to an all-pass filter, as illustrated in Figure 4B. Figure 4C displays the scattering parameter  $S_{21}$  through the metamaterial within a frequency range from 23 to 27 GHz. From the solid black curve obtained by EM simulation, the designed metamaterial exhibits strong filtering at the deployed state at roughly 25 GHz. At the folded state, there is over  $-5$  dB of transmission across the band, indicating that radiation can pass through the structure, denoted by the solid blue curve in Figure 4C. By structural reconfiguration through magnetic actuation, the EM metamaterial is able to switch between accepting and rejecting an incident wave. Experimental verification is carried out by fabricating a magnetic shape memory polymer-based metamaterial with attached periodic “S”-shaped patterns, as shown in Figure 4D. The fabricated

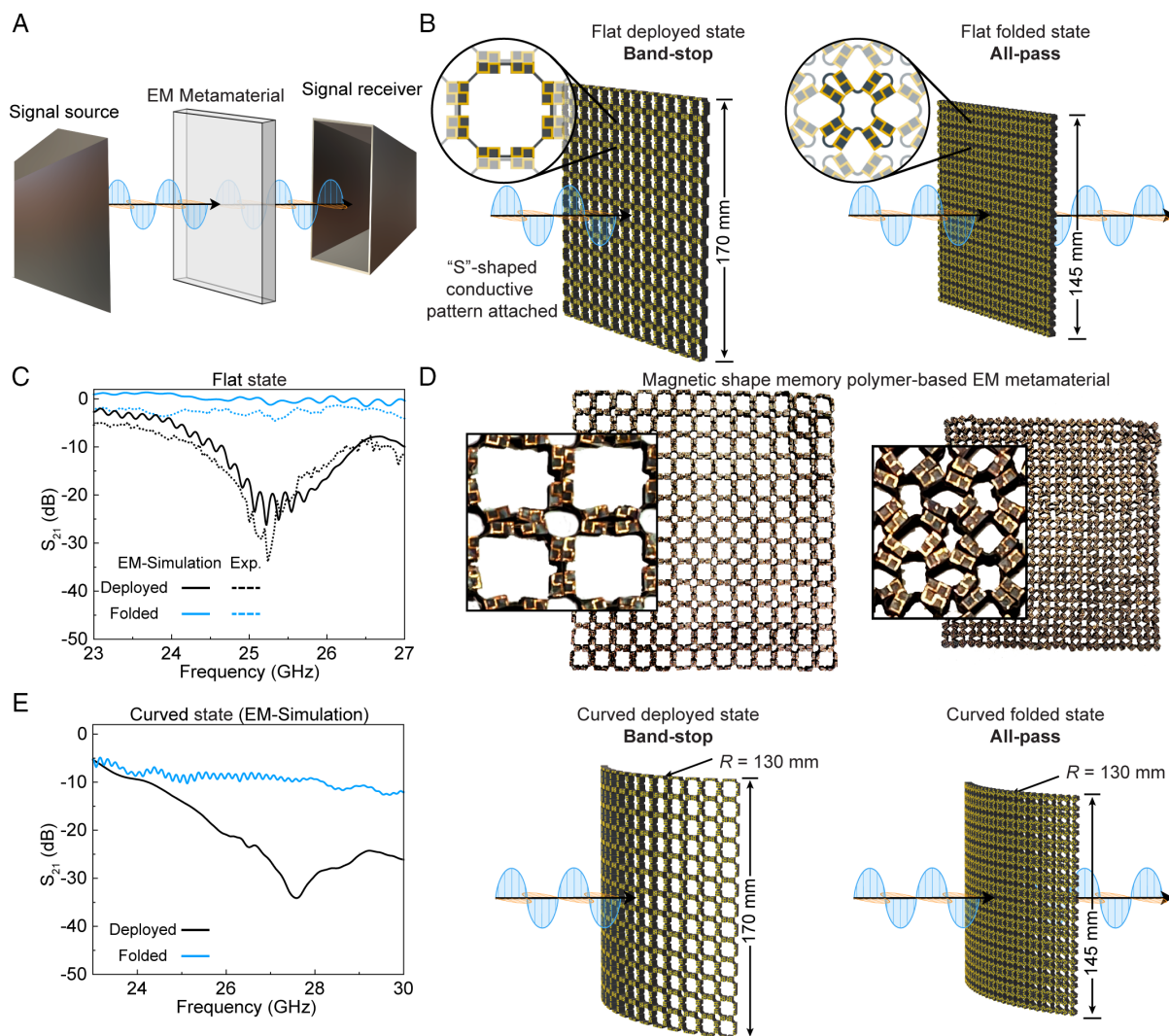


**Figure 4.** EM metamaterial with reconfigurable shape and EM properties. A) Full-wave model for the investigation of the metamaterial's EM behavior. B) Flat metamaterial with attached "S"-shaped conductive pattern as a reconfigurable filter. C) Full-wave EM prediction and experimental verification of the metamaterial's band-stop behavior at the deployed state and all-pass behavior at the folded state. D) Fabricated magnetic shape memory polymer metamaterial with shape-locking capability at deployed and folded states. E) Curved metamaterial attached with "S"-shaped conductive pattern as a reconfigurable EM filter.

structure demonstrates filtering at about 25 GHz at the deployed state (dotted black curve) and all-pass at the folded state (dotted blue curve) shown in Figure 4C, indicating good agreement with the prediction by EM simulation. It should be noted that the magnetic shape memory polymer used here is a composite whose stiffness can be tuned by temperature.<sup>[23]</sup> The material is soft and deformable at a high temperature and becomes stiff at room temperature to lock the deformed shape. The coupled thermal and magnetic actuation, together with the shape-locking capability, allows the metamaterial to reversibly reconfigure between the two EM behaviors without further consuming energy to maintain the deployed or folded states (Figure 4D). Conformability of the metamaterial is especially useful for curved structures such as an airplane wing. Our reported lattice-like metamaterial can easily conform to curved surfaces, and the EM performance at the

curved state is also studied via EM simulation, as shown in Figure 4E. The curved  $13 \times 13$  array with a radius of 130 mm behaves as an EM wave filter in the deployed state at 27.5 GHz denoted by the solid black curve and loses its filtering capability at the folded state (solid blue curve), demonstrating tunable EM behavior similar to the flat metamaterial.

## 2.5. Customizable Conductive Patterns for Tunable EM-Filtering Performance

The shape-morphing metamaterial can serve as the medium to structurally reconfigure and tune the EM behavior of different metamaterials, which are constructed by attaching various conductive patterns onto the unit. EM simulation is utilized to study the behaviors of infinite metamaterial carrying different

conductive patterns with periodic boundary conditions. Here, the dimensions of magnetic units are kept the same (Figure S6, Supporting Information). As shown in Figure 5A, “S”-shaped, “Z”-shaped, or dual-patch conductive patterns (yellow region) are designed and attached to the magnetic blocks (dark gray region), with an overall dimension of 1.5 mm by 3.2 mm and a space of 1.47 mm between two magnetic blocks. The widths of the fabricated “S”-shaped and “Z”-shaped are 0.3 mm. The width of each rectangle in the dual-patch pattern is 1.1 mm. The conductive patterns can be reconfigured by folding and deploying the metamaterial via magnetic actuation (Figure 5B). From the simulated  $S_{21}$  values shown in Figure 5C, the metamaterial shares the same all-pass behavior at the folded state (blue curves) but different filtering performances at the deployed state (black curves), presenting narrow-band, dual-band, and wide-band filtering behaviors for the “S”-shaped, “Z”-shaped, and dual-patch conductive patterns, respectively. The “S”-shaped pattern induces single filtering at 25.1 GHz with a peak value of  $-28$  dB and a relatively narrow bandwidth of 0.4 GHz (defined as  $S_{21}$  less than  $-15$  dB) in the range of 23–33 GHz. In the same frequency range, the “Z”-shaped pattern possesses two bands, located at 24.9 GHz with a peak value of  $-39$  dB and a bandwidth of 1 GHz and at 31.7 GHz with a peak value of  $-24$  dB and a bandwidth of 2 GHz. The dual-patch pattern shows a relatively wider band of 3.5 GHz, having the filtering effect from 28.1 to 31.6 GHz with a peak value of  $-53$  dB at 28.8 GHz. The results illustrate the

design flexibility of the magnetically reconfigurable EM metamaterial discussed in this work. This system can be further customized by changing the metamaterial design, either by designing a different base structure geometry or by altering the magnetization and hence the actuation. While three variations of a band-stop filter are presented, other filtering behaviors, such as band pass, can be achieved through the design of the metamaterial and functional conductive patterns.

### 3. Conclusion

In summary, we develop structurally reconfigurable EM metamaterials for tunable EM properties through magnetic actuation. The magnetic actuation enables reversible and fast shape morphing of the metamaterials between flat deployed, flat folded, curved deployed, and curved folded states in a programmable manner. By coupling local unit folding and global shape morphing, the metamaterials show excellent adaptability and design versatility. The metamaterials demonstrate conforming or 3D free-stand deforming to curved surfaces while maintaining EM property tunability. By introducing rationally designed conductive patterns onto the metamaterial surfaces, reconfigurable EM metamaterials can be constructed. The EM metamaterial can switch between accepting and rejecting incident EM waves. In addition, the structurally reconfigurable metamaterial serves as a medium for customizable conductive patterns to enlarge the

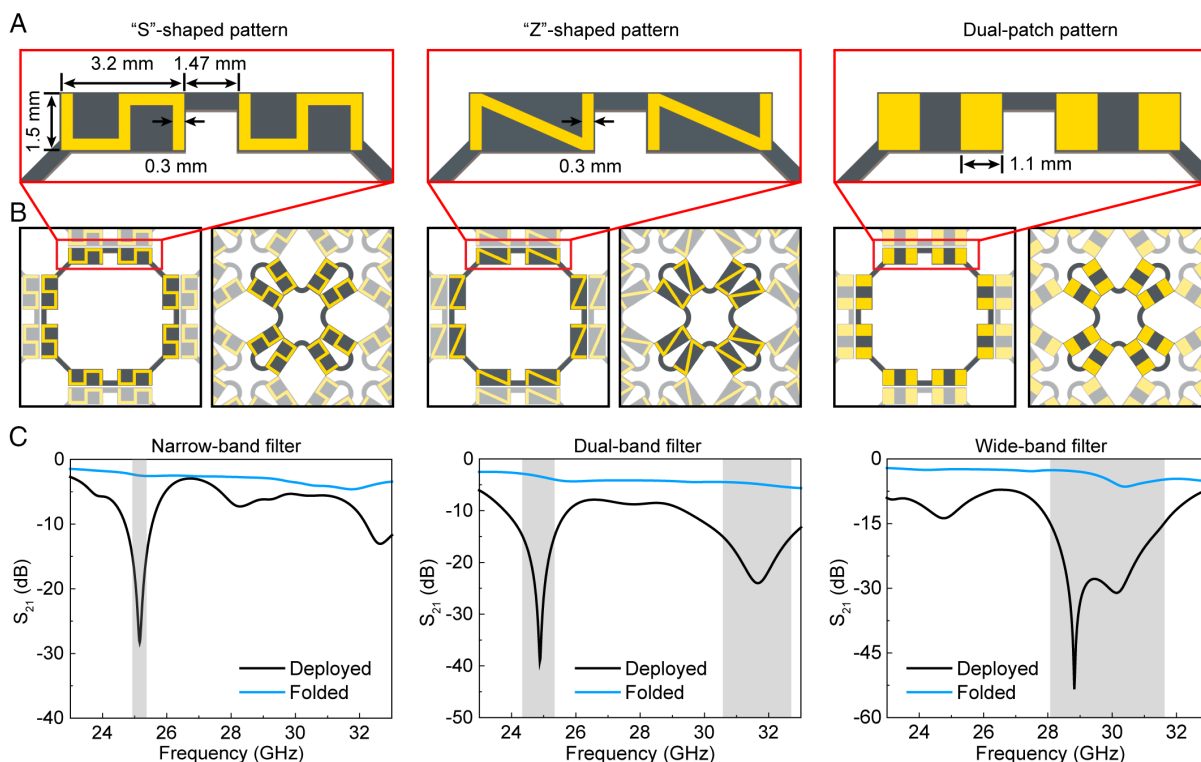


**Figure 5.** Reconfigurable EM metamaterial with varied filtering performance via customized conductive patterns. A) Geometries of subwavelength units with “S”-shaped, “Z”-shaped, and dual-patch patterns. B) Reconfigurations of the conductive patterns through metamaterial folding and deploying under the magnetic field. C) Simulated metamaterial’s performance with narrow-band, dual-band, and wide-band behaviors at the deployed state and all-pass at the folded state.

design space for a wide range of EM property tunabilities. Examples of the “S”-shaped, “Z”-shaped, and dual-patch conductive patterns demonstrated in this work show narrow-band, dual-band, and wide-band filtering behaviors. We anticipate the demonstrated design strategies enable next-generation reconfigurable EM metamaterials in defense and aerospace applications with enhanced programmability and adaptability.

## 4. Experimental Section

**Structural FEA:** Conformal shape morphing and freestanding actuation of the metamaterial were predicted utilizing commercial software ABAQUS 2020 (Dassault Systèmes, USA). A user-defined element subroutine (UEL) was adopted based on the neo-Hookean strain energy function coupled with magnetic potential.<sup>[24]</sup> Input parameters included the density of 2050 kg m<sup>-3</sup>, shear modulus of 50 kPa, bulk modulus of 5 MPa, magnetization of 80 kA m<sup>-1</sup> of the magnetic silicone-based metamaterial, and magnetic field. The substrate was treated as rigid material with surface-to-surface contact (friction coefficient of 0.3) to the metamaterial. The discrepancy of the magnetic field in structural FEA and experiments may be caused by unpredictable friction and geometry differences resulting from material fabrication.

**Magnetic Silicone-Based Metamaterial Fabrication:** Magnetic units were fabricated by mixing Ecoflex 00-30 (Smooth-On Inc., USA) and hard-magnetic particles (NdFeB, average size of 5 μm, Magnequench, Singapore) with a particle loading of 15 vol%. The mixture was degassed and then cured at 80 °C for 30 min in polyvinyl alcohol (PVA) molds 3D printed by Ultimaker S5 (Ultimaker, Netherlands). After dissolving soluble PVA molds in water, magnetic units were magnetized with specific in-plane/out-of-plane magnetizations under a 1.5 T impulse magnetic field by an in-house built magnetizer. Based on the predetermined local/global magnetization distribution, magnetic units were assembled and glued together using Sil-poxy adhesive (Smooth-On Inc., USA).

**Electromagnetic Simulations:** The EM metamaterial performance was simulated using the CST Microwave Studio (Dassault Systèmes, USA). Time-domain (transient) solver was used for a finite array. However, initially, the EM metamaterial units with predetermined conductive patterns were simulated using periodic boundary conditions with the frequency domain solver, simulating an infinitely periodic structure to get the ideal behavior of a specific design. In practice, a finite structure inherently diverged from this performance, but a larger number of metamaterial units approximated more closely to the ideal case. A 13×13 EM metamaterial was sufficiently large to represent an infinite metamaterial and was easy to fabricate. For the finite metamaterial performance simulation, the CST time-domain solver was used. The EM metamaterial at either deployed or folded state was modeled between two horn antennas 1.4 m apart to mimic the measurement setup. Multiple experimental measurements were performed to characterize the magnetic shape memory polymer-based metamaterial, obtaining a relative permittivity of 6.3 ± 1.3 and loss tangent of 0.07. The relative permittivity of 6.3 and loss tangent of 0.07 were used for the EM simulations producing filtering of the deployed metamaterial at the experimentally verified frequency.

**Magnetic Shape Memory Polymer-Based Metamaterial Fabrication:** The shape memory polymer was an acrylate-based polymer containing aliphatic urethane diacrylate (Ebecryl 8413, Allnex, USA), isobornyl acrylate (Sigma-Aldrich, USA), and 2-phenoxyethanol acrylate (Ebecryl 114, Allnex, USA), mixed in a weight ratio of 10:60:30. 0.4 wt% thermal initiator 2,2'-Azobis(2-methylpropionitrile) (Sigma-Aldrich, USA) was added to enable thermal curing and 2 wt% fumed silica (200 nm, Sigma-Aldrich, USA) was used to ensure homogeneous particle dispersion. The polymer precursor was mixed with hard-magnetic particles with a particle loading of 20 vol% and degassed before further molding. The mixture was poured into the PVA molds and cured at 80 °C for 4 h and post-processed at 120 °C for 30 min. Shape memory polymer-based magnetic units were then magnetized and glued into an array by pure shape memory polymer. “S”-shaped conductive patterns were cut from a 40 μm-thick copper tape using a

355 nm UV Laser Marking System (DPSS Laser Inc., USA) with laser power of 3 W, scan rate of 100 mm s<sup>-1</sup>, frequency of 70 kHz, and 65 passes. The conductive patterns were attached to the metamaterial for EM behavior measurement.

**Electromagnetic Metamaterial Filtering Effect Characterization:** To characterize the EM metamaterials, two linearly polarized horn antennas were connected to a network analyzer (Anritsu Corporation, Japan) and directed toward each other. A reference transmission measurement was taken without the EM metamaterial between the horn antennas to characterize attenuation and path loss. Next, measurements were carried out with the reconfigurable EM metamaterial placed between the horn antennas at the folded and deployed states. The reference measurement was subtracted from the measurements with the metamaterial to isolate the structure's behavior.

## Supporting Information

Supporting Information is available from the Wiley Online Library or from the author.

## Acknowledgements

S.W., J.E., and J.D. contributed equally to this work. R.R.Z., S.W., J.D., and Y.C. acknowledge support from NSF Career Award CMMI-2145601 and NSF Award CMMI-2142789. N.G., J.E. acknowledges support from Consortium on Electromagnetics and Radio Frequencies. The authors thank Sophie Leanza for her insightful discussions that improved the manuscript. The Interactive Supporting Information of this article can be found at: <https://www.authorea.com/doi/full/10.22541/au.165478179.98256479>.

## Conflict of Interest

The authors declare no conflict of interest.

## Data Availability Statement

The data that support the findings of this study are available from the corresponding author upon reasonable request.

## Keywords

active metamaterials, conformal metamaterials, electromagnetic filters, magnetic actuation, magnetic shape memory polymers

Received: May 2, 2022

Revised: June 8, 2022

Published online: July 7, 2022

- [1] a) K. Bertoldi, V. Vitelli, J. Christensen, M. Van Hecke, *Nat. Rev. Mater.* **2017**, 2, 1; b) J. U. Surjadi, L. Gao, H. Du, X. Li, X. Xiong, N. X. Fang, Y. Lu, *Adv. Eng. Mater.* **2019**, 21, 1800864; c) Z. Zhai, L. Wu, H. Jiang, *Appl. Phys. Rev.* **2021**, 8, 041319.
- [2] a) G. Ma, P. Sheng, *Sci. Adv.* **2016**, 2, e1501595; b) B. Assouar, B. Liang, Y. Wu, Y. Li, J.-C. Cheng, Y. Jing, *Nat. Rev. Mater.* **2018**, 3, 460; c) H. Nassar, B. Yousefzadeh, R. Fleury, M. Ruzzene, A. Alù, C. Daraio, A. N. Norris, G. Huang, M. R. Haberman, *Nat. Rev. Mater.* **2020**, 5, 667.
- [3] J. Jiang, M. Chen, J. A. Fan, *Nat. Rev. Mater.* **2021**, 6, 679.
- [4] G. Duan, X. Zhao, S. W. Anderson, X. Zhang, *Commun. Phys.* **2019**, 2, 1.



- [5] G. Ma, M. Yang, Z. Yang, P. Sheng, *Appl. Phys. Lett.* **2013**, *103*, 011903.
- [6] Y. Li, E. Baker, T. Reissman, C. Sun, W. K. Liu, *Appl. Phys. Lett.* **2017**, *111*, 251903.
- [7] T. Phan, D. Sell, E. W. Wang, S. Doshay, K. Edee, J. Yang, J. A. Fan, *Light: Sci. Appl.* **2019**, *8*, 1.
- [8] S. Zhang, C. Xia, N. Fang, *Phys. Rev. Lett.* **2011**, *106*, 024301.
- [9] X. Xu, Q. Wu, Y. Pang, Y. Cao, Y. Fang, G. Huang, C. Cao, *Adv. Funct. Mater.* **2022**, *32*, 2107896.
- [10] a) J. D. Ortiz, J. D. Baena, V. Losada, F. Medina, R. Marques, J. A. Quijano, *IEEE Microwave Wireless Compon. Lett.* **2013**, *23*, 291; b) F.-C. Huang, C.-N. Chiu, T.-L. Wu, Y.-P. Chiou, *ITEIC* **2015**, *57*, 365; c) N. Nasimuddin, Z. N. Chen, X. Qing, *IEEE Antennas Propag. Mag.* **2016**, *58*, 39.
- [11] a) A. Iniguez-Rabago, Y. Li, J. T. Overvelde, *Nat. Commun.* **2019**, *10*, 1; b) Y. Wang, L. Li, D. Hofmann, J. E. Andrade, C. Daraió, *Nature* **2021**, *596*, 238; c) T. Chen, M. Pauly, P. M. Reis, *Nature* **2021**, *589*, 386; d) S. M. Montgomery, S. Wu, X. Kuang, C. D. Armstrong, C. Zemelka, Q. Ze, R. Zhang, R. Zhao, H. J. Qi, *Adv. Funct. Mater.* **2021**, *31*, 2005319; e) S. Wu, Q. Ze, J. Dai, N. Udipi, G. H. Paulino, R. Zhao, *Proc. Natl. Acad. Sci.* **2021**, *118*, e2110023118; f) L. Kang, Q. Zhao, H. Zhao, J. Zhou, *Opt. Express* **2008**, *16*, 8825.
- [12] a) Z. Guanxing, Z. Liu, W. Deng, W. Zhu, *JOpt* **2020**, *23*, 013001; b) S. Xiao, T. Wang, T. Liu, C. Zhou, X. Jiang, J. Zhang, *J. Phys. D: Appl. Phys.* **2020**, *53*, 503002.
- [13] J. Hu, G. Q. Luo, Z.-C. Hao, *IEEE Access* **2017**, *6*, 6130.
- [14] a) B. Ratni, A. de Lustrac, G.-P. Piau, S. N. Burokur, *Appl. Phys. Lett.* **2017**, *111*, 214101; b) X. Gao, W. L. Yang, H. F. Ma, Q. Cheng, X. H. Yu, T. J. Cui, *IEEE Trans. Antennas Propag.* **2018**, *66*, 6086.
- [15] H. L. Wang, H. F. Ma, M. Chen, S. Sun, T. J. Cui, *Adv. Funct. Mater.* **2021**, *31*, 2100275.
- [16] a) B. Ghassemiparvin, N. Ghalichechian, *JMemS* **2020**, *29*, 621; b) M. Lust, S. Chen, C. E. Wilson, J. Argo, V. Doan-Nguyen, N. Ghalichechian, *J. Appl. Phys.* **2020**, *127*, 205303.
- [17] a) D. Kim, R. G. Pierce, R. Henderson, S. J. Doo, K. Yoo, J.-B. Lee, *Appl. Phys. Lett.* **2014**, *105*, 234104; b) M. Odit, P. Kapitanova, A. Andryeuskii, P. Belov, A. V. Lavrinenko, *Appl. Phys. Lett.* **2016**, *109*, 011901; c) C. Ni, M. S. Chen, Z. X. Zhang, X. L. Wu, *IEEE Antennas Wireless Propag. Lett.* **2017**, *17*, 78; d) J. Eichenberger, N. Ghalichechian, *IEEE Antennas Wireless Propag. Lett.* **2021**, *20*, 2048; e) K. Q. Henderson, N. Ghalichechian, presented at 2020 14th European Conference on Antennas and Propagation (EuCAP), Copenhagen, Denmark, 2020.
- [18] S. I. H. Shah, S. Lim, *Mater. Des.* **2021**, *198*, 109345.
- [19] a) X. Liu, S. Yao, B. S. Cook, M. M. Tentzeris, S. V. Georgakopoulos, *IEEE Trans. Antennas Propag.* **2015**, *63*, 5897; b) Z. Wang, L. Jing, K. Yao, Y. Yang, B. Zheng, C. M. Soukoulis, H. Chen, Y. Liu, *Adv. Mater.* **2017**, *29*, 1700412; c) Y. Zheng, K. Chen, W. Yang, L. Wu, K. Qu, J. Zhao, T. Jiang, Y. Feng, *Adv. Funct. Mater.* **2022**, *32*, 2107699; d) X. Zhang, J. Ma, M. Li, Z. You, X. Wang, Y. Luo, K. Ma, Y. Chen, *Proc. Natl. Acad. Sci.* **2022**, *119*, e2117649119.
- [20] a) S. Lee, S. Kim, T. T. Kim, Y. Kim, M. Choi, S. H. Lee, J. Y. Kim, B. Min, *Adv. Mater.* **2012**, *24*, 3491; b) Y. Zárate, S. Babae, S. H. Kang, D. N. Neshev, I. V. Shadrivov, K. Bertoldi, D. A. Powell, *Sci. Rep.* **2016**, *6*, 1; c) F. Liu, Y. Chen, H. Song, F. Zhang, Z. Fan, Y. Liu, X. Feng, J. A. Rogers, Y. Huang, Y. Zhang, *Small* **2019**, *15*, 1804055; d) K. Bai, X. Cheng, Z. Xue, H. Song, L. Sang, F. Zhang, F. Liu, X. Luo, W. Huang, Y. Huang, *Sci. Adv.* **2020**, *6*, eabb7417.
- [21] a) M. Lapine, I. V. Shadrivov, D. A. Powell, Y. S. Kivshar, *Nat. Mater.* **2012**, *11*, 30; b) J. Valente, J.-Y. Ou, E. Plum, I. J. Youngs, N. I. Zheludev, *Appl. Phys. Lett.* **2015**, *106*, 111905; c) J. Valente, J.-Y. Ou, E. Plum, I. J. Youngs, N. I. Zheludev, *Nat. Commun.* **2015**, *6*, 1.
- [22] a) S. Wu, Q. Ze, R. Zhang, N. Hu, Y. Cheng, F. Yang, R. Zhao, *ACS Appl. Mater. Interfaces* **2019**, *11*, 41649; b) Y. Alapan, A. C. Karacakol, S. N. Guzelhan, I. Isik, M. Sitti, *Sci. Adv.* **2020**, *6*, eabc6414; c) H. Gu, Q. Boehler, D. Ahmed, B. J. Nelson, *Sci. Rob.* **2019**, *4*, eaax8977.
- [23] a) C. Ma, S. Wu, Q. Ze, X. Kuang, R. Zhang, H. J. Qi, R. Zhao, *ACS Appl. Mater. Interfaces* **2020**, *13*, 12639; b) Q. Ze, X. Kuang, S. Wu, J. Wong, S. M. Montgomery, R. Zhang, J. M. Kovitz, F. Yang, H. J. Qi, R. Zhao, *Adv. Mater.* **2020**, *32*, 1906657.
- [24] R. Zhao, Y. Kim, S. A. Chester, P. Sharma, X. Zhao, *J. Mech. Phys. Solids* **2019**, *124*, 244.